

# Alternant Hydrocarbon Diradicals as Optically Addressable Molecular Qubits

Yong Rui Poh,<sup>1</sup> Dmitry Morozov,<sup>2</sup> Nathanael P. Kazmierczak,<sup>3</sup>  
Ryan G. Hadt,<sup>3,\*</sup> Gerrit Groenhof,<sup>4,†</sup> and Joel Yuen-Zhou<sup>1,‡</sup>

<sup>1</sup>Department of Chemistry and Biochemistry, University of California San Diego, La Jolla, California 92093, USA

<sup>2</sup>Terra Quantum AG, Kornhausstrasse 25, 9000 St. Gallen, Switzerland

<sup>3</sup>Division of Chemistry and Chemical Engineering,

Arthur Amos Noyes Laboratory of Chemical Physics,

California Institute of Technology, Pasadena, California 91125, USA

<sup>4</sup>Nanoscience Center and Department of Chemistry, University of Jyväskylä, Jyväskylä, Finland

(Dated: March 13, 2024)

High-spin molecules allow for bottom-up qubit design and are promising platforms for magnetic sensing and quantum information science. Optical addressability of molecular electron spins has also been proposed in first-row transition metal complexes via optically-detected magnetic resonance (ODMR) mechanisms analogous to the diamond-NV colour centre. However, significantly less progress has been made on the front of metal-free molecules, which can deliver lower costs and milder environmental impacts. At present, most luminescent open-shell organic molecules are  $\pi$ -diradicals, but such systems often suffer from poor ground-state open-shell characters necessary to realise a stable molecular qubit. In this work, we propose the use of alternancy symmetry to selectively minimise radical-radical interactions in the ground state, generating  $\pi$ -systems with high diradical characters. We call them *m*-dimers, referencing the need to covalently link two benzylic radicals at their *meta* carbon atoms for the desired symmetry. Through a detailed electronic structure analysis, we find that the excited states of alternant hydrocarbon *m*-diradicals contain important symmetries that can be used to construct ODMR mechanisms. The molecular parameters are set in the context of a tris(2,4,6-trichlorophenyl)methyl (TTM) radical dimer covalently tethered at the *meta* position, demonstrating the feasibility of realising a molecular colour centre with alternant  $\pi$ -diradicals.

## I. INTRODUCTION

There has been sustained interest in designing optically addressable electron spins that can be both initialised (polarised) and read out by optical means [1]. Known as optically-detected magnetic resonance (ODMR), this technique offers precise control of a single qubit and has found numerous applications in quantum sensing [2] and quantum information science [3]. The platform, referred to as a colour centre, is often a solid-state spin defect such as a nitrogen-vacancy (NV) centre in diamond [4–8]. However, because these defects are introduced post-synthesis and often without control over their locations, defect-based colour centres suffer from poor scalability and tunability.

These problems can be tackled with molecular spin systems because they can be synthesised from bottom-up and extended into macromolecular systems [9–13]. Metal complexes have seen the most advancements, particularly with transition metals [14–25]. By contrast, little progress has been made with fully organic molecules [26–30] which, being metal-free, will be more cost-efficient and sustainable than their metal-based counterparts. Following the pioneering work of Gorgon et al. in synthesising an optically-addressable organic colour centre [27], we present the first theoretical analysis on the spin-optical interface of such systems.

In diamond-NV centres, ODMR is achieved via the following procedure [31]: Upon photoexcitation of the triplet ground state to the excited state (also a triplet), intersystem crossing (ISC) to a singlet excited state occurs with a change in magnetic quantum number  $M_S$ . This increases the relative population of the excited triplet  $M_S = 0$  level, the photoluminescence (PL) of which transfers the spin polarisation to the ground state (optical initialisation). The PL

intensity also indicates the ground state polarisation (optical readout). As for the singlet excited state, its population decays non-radiatively to the triplet  $M_S = 0$  ground state, its irreversibility being the key towards overall purification of the ground state spins [Fig. 1a]. There are thus three elements to engineer in a metal-free molecular system: (1) A high-spin ground state, (2) spin-selective interactions among the excited states, and (3) irreversible relaxation to the ground state.

Element (1) suggests the use of an organic diradical. Thus far, most luminescent diradicals have involved some degree of  $\pi$ -conjugation [32–39], which has proven useful in the chemical assembly of spin arrays [33]. However, large spatial separation between the two paramagnetic centres is often necessary to minimise radical-radical interactions and achieve a high-spin ground state [Fig. 1b] [40–43]. In most cases, this separation extends to the excited states as well, which is disadvantageous for element (2). Indeed, in Gorgon et al.’s seminal work, interradical interaction was achieved via a charge transfer to the spacer’s triplet state, generating a complicated manifold of 12 coupled electronic levels [27]. To avoid this issue, future designs may reduce (improve) the stability of the molecule’s closed-shell (open-shell) Kekulé structures, with a crude measure being the number of Clar sextets minus the number of unpaired electrons [44]. In some extreme cases,  $\pi$ -diradicals may have no closed-shell Kekulé structures at all; such molecules are termed “non-Kekulé” [40, 43] and an example has been shown in Fig. 1c. However, this analysis is purely qualitative and there exist non-Kekulé molecules with appreciable closed-shell characters [42]. (Interestingly, alkaline earth metal complexes [45], commonly used as optical cycling centres [46, 47], as well as nitrenes [48] have also been investigated for luminescent diradical properties and are useful candidates of molecular colour centres as well.)

Alternant hydrocarbon radicals (AHRs) are a special type of hydrocarbon  $\pi$ -electron radicals. In AHRs, atoms contributing to the  $\pi$  framework may be divided into two classes such that no two atoms from the same class are adjacent [Fig. 1d]. Importantly, within Hückel theory of nearest-neighbour hopping, the singly occupied molecular orbital

\* rghadt@caltech.edu

† gerrit.x.groenhof@jyu.fi

‡ joelyuen@ucsd.edu

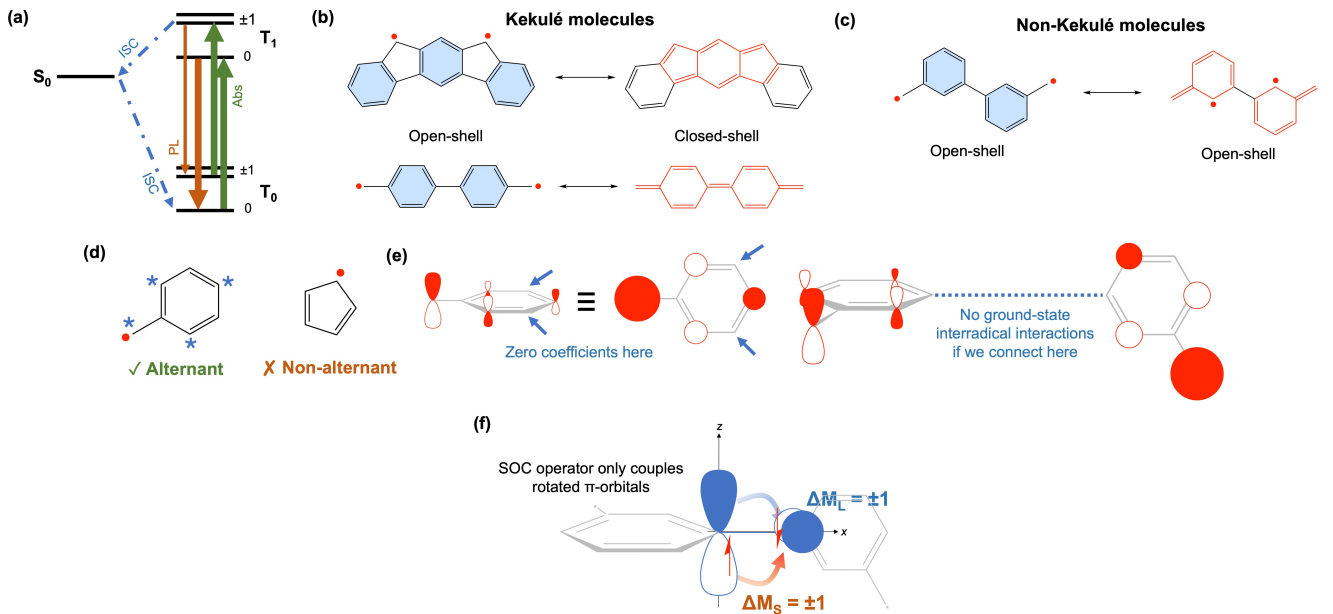


**FIG. 1:** (a) Colour centres like diamond-NV defects can be spin polarised by multiple photoexcitation (Abs) cycles, the intensity of PL being an indicator of the ground-state spin polarisation. This procedure is known as ODMR. (b) Kekulé hydrocarbons are conjugated  $\pi$ -systems with at least one closed-shell Kekulé structure. These molecules tend to have lower diradical characters. (c) Non-Kekulé structures have no closed-shell Kekulé structures and are hence more likely to have open-shell ground states. (d) Alternant hydrocarbons are  $\pi$ -systems whereby the  $\pi$ -contributing atoms may be divided into two classes, starred [\*] and unstarred [ ], such that no two atoms from the same class are adjacent. (e) Within the Hückel framework, radicals constructed with alternacy symmetry (termed AHRs) have their SOMOs localised on the starred atoms (the class with more atoms). As such, two AHRs covalently bonded via the unstarred atoms will have vanishing radical-radical interactions. These molecules are non-Kekulé, as shown in (c). (f) In  $\pi$ -electron systems, SOC-mediated ISC can only occur between rotated  $\pi$ -orbitals, in line with the El-Sayed rules. Due to conservation of angular momentum, an electron spin flip must occur concomitantly, making a triplet-singlet ISC process spin-selective.

(SOMO) is localised on atoms from only one class – the class containing more atoms [Fig. 1e]. As such, by covalently tethering two AHRs via atoms of the *other* class, radical-radical interactions may be avoided in the ground state, that is, the resulting diradical is non-Kekulé and quantitatively predicted to be open-shell within the Hückel framework. Note that interradical interactions are retained in the excited states because the occupied and virtual molecular orbitals (MOs) are in general delocalised across both atom classes; this is necessary for element (2).

Thus far, we have not addressed the spin selectivity component of element (2). This was achieved in NV centres via an ISC process mediated by spin-orbit coupling (SOC) [31], but these rates are negligible if the  $\pi$ -conjugated system is fully planar. The reason may be found in the SOC operator, which in its mean-field Breit-Pauli form has the structure of  $\hat{\mathbf{L}} \cdot \hat{\mathbf{S}} = \hat{L}_z \hat{S}_z + \hat{L}_+ \hat{S}_{-}/2 + \hat{L}_{-} \hat{S}_{+}/2$ , where  $\hat{\mathbf{L}}$  and  $\hat{\mathbf{S}}$  are the orbital and spin angular momentum vector operators respectively [49]. The first operator vanishes when acting on  $2p_z$  atomic orbitals (AOs), while the other two operators rotate  $2p_z$  orbitals into linear combinations of  $2p_x$  and  $2p_y$  orbitals. Therefore, the SOC operator only connects between rotated  $2p$  (or  $\pi$ ) orbitals [Fig. 1f]. This is essentially the statement of El-Sayed [50] and implies that torsion between the radical  $\pi$ -systems is important for element (2) [51–54]. Finally, since orbital rotation constitutes a  $\Delta M_L = \pm 1$  transition, to conserve total angular momentum the spin must also change by  $\Delta M_S = \pm 1$ , giving rise to the spin selectivity of ISC in  $\pi$ -electron systems [51, 53, 54].

Therefore, through a qualitative analysis, we find potential in realising an NV centre analogue by attaching two AHRs covalently at selected atoms and with significant torsion. We call them AHR *m*-dimers, referencing the fact that

most luminescent  $\pi$ -radicals have benzylic structures and thus should be dimerised via atoms at the *meta* position. In this work, we make further progress by analysing the electronic structure of AHR *m*-dimers and the symmetries of their excited wavefunctions. By adopting a mean-field approach to the Pariser-Parr-Pople (PPP) model [55–57] (also known as the extended Hubbard model), we find that not all excitations are emissive and only few within the subset can undergo triplet-singlet ISC. This makes the excited state kinetics highly selective and useful for generating robust ODMR mechanisms. These observations are set in the context of two existing AHRs – a methylated benzylic radical and the tris(2,4,6-trichlorophenyl)methyl (TTM) radical – using parameters estimated from density functional theory (DFT), further demonstrating the possibility of designing a molecular colour center with AHR *m*-dimers. For the methylated benzylic radical, our DFT-parametrised excited states also matched the results from a multi-configurational level of theory.

The paper is organised as such: In Sec. II A, the electronic structure of AHR *m*-dimers is analysed using the PPP framework. This section is technical and the reader may safely skip it at the first pass. In Sec. II B, ODMR mechanisms are proposed based on results from the PPP model. In Sec. II C, the PPP predictions are verified by ab initio calculations. Finally, in Sec. II D, a mapping between a polarised ground-state triplet and an operational qubit is proposed.

## II. RESULTS AND DISCUSSIONS

### A. Electronic structure analysis

The PPP model [55–57] is an extension of the Hückel model to include additional Coulomb interactions. It partially resolves the electron-electron correlation problem and continues to be the reference model for  $\pi$ -conjugated hydrocarbons. By considering only the minimal basis of  $2p$  AOs that constitute the  $\pi$ -electron system, the PPP Hamiltonian reads

$$\hat{H}_{\text{PPP}} = \sum_{\mu} \alpha_{\mu} \hat{n}_{\mu} - \sum_{\langle \nu > \mu \rangle} \sum_{\sigma} \beta_{\mu\nu} (\hat{a}_{\mu\sigma}^{\dagger} \hat{a}_{\nu\sigma} + \hat{a}_{\nu\sigma}^{\dagger} \hat{a}_{\mu\sigma}) + \sum_{\mu} \gamma_{\mu\mu} \hat{n}_{\mu\alpha} \hat{n}_{\mu\beta} + \sum_{\nu > \mu} \gamma_{\mu\nu} \hat{n}_{\mu} \hat{n}_{\nu}, \quad (1)$$

with  $\hat{a}_{\mu\sigma}^{\dagger}$  ( $\hat{a}_{\mu\sigma}$ ) being the fermionic creation (annihilation) operator for an electron in the  $2p$  AO of atom  $\mu$  with spin  $\sigma$  ( $= \alpha, \beta$ ),  $\hat{n}_{\mu\sigma} \equiv \hat{a}_{\mu\sigma}^{\dagger} \hat{a}_{\mu\sigma}$  being the number operator and  $\hat{n}_{\mu} \equiv \sum_{\sigma=\alpha, \beta} \hat{n}_{\mu\sigma}$ . Here, we have used  $\alpha$  ( $\beta$ ) to denote spin-up (spin-down) electrons. The parameters are defined as followed:  $\alpha_{\mu}$  is the on-site energy of atom  $\mu$ ,  $\beta_{\mu\nu}$  is the hopping amplitude between atoms  $\mu$  and  $\nu$ , and  $\gamma_{\mu\nu}$  represents the effective Coulombic repulsion between an electron on atom  $\mu$  and another electron on atom  $\nu$ . Finally,  $\langle \cdot \rangle$  denotes nearest neighbours.

Its application towards AHRs was explored by Longuet-Higgins and Pople using a mean-field approach similar to Hartree-Fock theory [58–60]. The results remain qualitatively the same as the Hückel approach, that is, if we label the alternacy class containing more atoms by stars [\*] [Fig. 1d], then each HOMO- $j$  has the same atomic coefficients as the corresponding LUMO+ $j$ , except with opposite signs on the unstarred atoms. This is known as the pairing theorem and, consequently, the SOMO has nodes on the unstarred atoms. An excellent review on this topic has been provided by Hele [61] and we shall not rederive the results. Instead, we will briefly mention that, within the aforementioned mean-field treatment, the AHR's electronic ground state (GS) is a doublet described by the following (Slater) determinants:

$$|\Psi; +1/2\rangle = |\cdots 2\bar{2}1\bar{1}0\rangle, \quad |\Psi; -1/2\rangle = |\cdots 2\bar{2}1\bar{1}0\rangle, \quad (2)$$

that is, determinants with one electron in the SOMO ( $j = 0$ ) and two electrons in each HOMO- $j$  ( $j = 1, 2, \dots$ ). In this work, we shall follow standard electronic structure theory notation [62]. In addition, the second state index labels the spin magnetic number  $M_S \in \{+1/2, -1/2\}$ .

Yet another consequence of alternacy symmetry is the invariance of  $\hat{H}_{\text{PPP}}$  [Eq. (1)] under particle-hole transformation (PHT)  $\hat{a}_{\mu\sigma}^{\dagger} \rightarrow f_{\mu} \hat{a}_{\mu\bar{\sigma}}$  with  $f_{\mu}$  being  $+1$  if  $\mu$  is starred and  $-1$  otherwise ( $\bar{\sigma}$  is the spin complementary to  $\sigma$ ). As such, it is apt to label electronic states of AHRs by their symmetries under PHT, be it odd or even. For instance, when considering an  $\alpha$ -spin excitation from SOMO to LUMO+ $j$ , labelled  $|\Psi_0^{j'}; +1/2\rangle$ , one should take a linear combination with the  $\beta$ -spin HOMO- $j$  to SOMO transition  $|\Psi_j^0; +1/2\rangle$ , which is related to the latter by PHT, such that the resulting state has a well-defined symmetry under PHT. Following the notation set by Pariser [63, 64], we label these symmetry-adapted states by “+” and “-” representing symmetric and antisymmetric combinations respectively:

$$|\Psi_{0j}^{\pm}; +1/2\rangle \equiv \frac{|\Psi_j^0; +1/2\rangle \pm |\Psi_0^{j'}; +1/2\rangle}{\sqrt{2}}. \quad (3)$$

We note that due to differences in origin (Pariser was considering configuration interactions), some “+” states may

be odd (instead of even) under PHT and the same can happen to “-” states too. Despite that, there is a one-to-one mapping between the two notations, justifying our choice of Pariser's (see Supplementary Information S1).

Our  $m$ -dimer system comprises two AHRs covalently tethered via the unstarred atoms (the class containing fewer atoms) [Fig. 2a]. The entire  $\pi$ -electron system is modelled by the PPP Hamiltonian. Because the monomers are rotated relative to each other by sterics, any intermonomer couplings due to  $\pi$ -orbital overlaps may be treated perturbatively. As such, we partition the Hamiltonian into monomeric components:

$$\hat{H}_r = \sum_{\mu \in \mathcal{N}_r} \alpha_{\mu} \hat{n}_{\mu} - \sum_{\langle \nu > \mu \in \mathcal{N}_r \rangle} \sum_{\sigma} \beta_{\mu\nu} (\hat{a}_{\mu\sigma}^{\dagger} \hat{a}_{\nu\sigma} + \hat{a}_{\nu\sigma}^{\dagger} \hat{a}_{\mu\sigma}) + \sum_{\mu \in \mathcal{N}_r} \gamma_{\mu\mu} \hat{n}_{\mu\alpha} \hat{n}_{\mu\beta} + \sum_{\nu > \mu \in \mathcal{N}_r} \gamma_{\mu\nu} \hat{n}_{\mu} \hat{n}_{\nu}, \quad (4)$$

and perturbative intermonomer couplings:

$$\hat{V}_{AB} = - \sum_{\langle \mu \in \mathcal{N}_A, \nu \in \mathcal{N}_B \rangle} \sum_{\sigma} \beta_{\mu\nu} (\hat{a}_{\mu\sigma}^{\dagger} \hat{a}_{\nu\sigma} + \hat{a}_{\nu\sigma}^{\dagger} \hat{a}_{\mu\sigma}) + \sum_{\mu \in \mathcal{N}_A, \nu \in \mathcal{N}_B} \gamma_{\mu\nu} \hat{n}_{\mu} \hat{n}_{\nu}, \quad (5)$$

such that the full Hamiltonian reads  $\hat{H} = \hat{H}_A + \hat{H}_B + \hat{V}_{AB}$ . Here,  $r \in \{A, B\}$  labels the two monomers and  $\mathcal{N}_r$  denotes the set of atoms in monomer  $r$ .

Before solving the Hamiltonian  $\hat{H}$ , it is useful to understand the types of electronic states to expect. We note that all dimers have a  $C_2$  rotational symmetry and both  $\hat{H}_A + \hat{H}_B$  and  $\hat{V}_{AB}$  are symmetric under this transformation. Furthermore, the  $m$ -dimer is also alternant so both  $\hat{H}_A + \hat{H}_B$  and  $\hat{V}_{AB}$  are symmetric under PHT as well. As such, focusing on the zeroth-order term  $\hat{H}_A + \hat{H}_B$  for now, the zeroth-order electronic states may be organised by eigenvalues of the molecule's spin and symmetry operators, namely (1) the spin numbers,  $S$  and  $M_S$ , (2) symmetry under PHT,  $P \in \{+, -\}$ , and (3) irreducible representations (irreps) of the  $C_2$  point group,  $\Gamma \in \{A, B\}$ , presented in typewriter font to avoid confusion with the monomer index. In this work, we packed them into the following notation for electronic states:

$$|^{2S+1}\Phi_{\Gamma}^{jk, P}; M_S \rangle, \quad (6)$$

with  $\Phi$  labelling the class of excitation and  $\{j, k\}$  labelling the MOs involved in the excitation (more to follow).

To solve the Hamiltonian, we note that the monoradical terms  $\hat{H}_A$  and  $\hat{H}_B$  each admit the same mean-field solutions as those obtained by Longuet-Higgins and Pople, described by Eq. (2). As such, because the two monomers are non-interacting at  $\hat{V}_{AB} = 0$ , the approximate zeroth-order electronic ground states ( $\Phi = \text{GS}$ ) to the full zeroth-order Hamiltonian  $\hat{H}_A + \hat{H}_B$  will be (tensor) products of the monoradical's mean-field solutions. This yields a singlet state  $|^1\text{GS}; 0\rangle$  and a set of triplet states  $\{|^3\text{GS}; M_S\rangle | M_S = -1, 0, +1\}$ , all of which have “-” particle-hole symmetry. Note that we continue to use the basis of MOs localised on each monomer; for instance,  $|^3\text{GS}; +1\rangle = |\cdots 1_A \bar{1}_A 0_A \cdots 1_B \bar{1}_B 0_B\rangle$ , with  $j_r$  being the  $j$ -th MO of monomer  $r$ .

As for the zeroth-order low-lying excited states, they are approximated by single excitations from the GS, just like the monoradical case [Eq. (3)]. With dimers, there can be two types of excited states: local excitations ( $\Phi = \text{LE}$ ), which move electrons within the same monomer, and charge transfers ( $\Phi = \text{CT}$ ), which excite electrons to the other monomer. Fig. 2b provides a diagrammatic representation

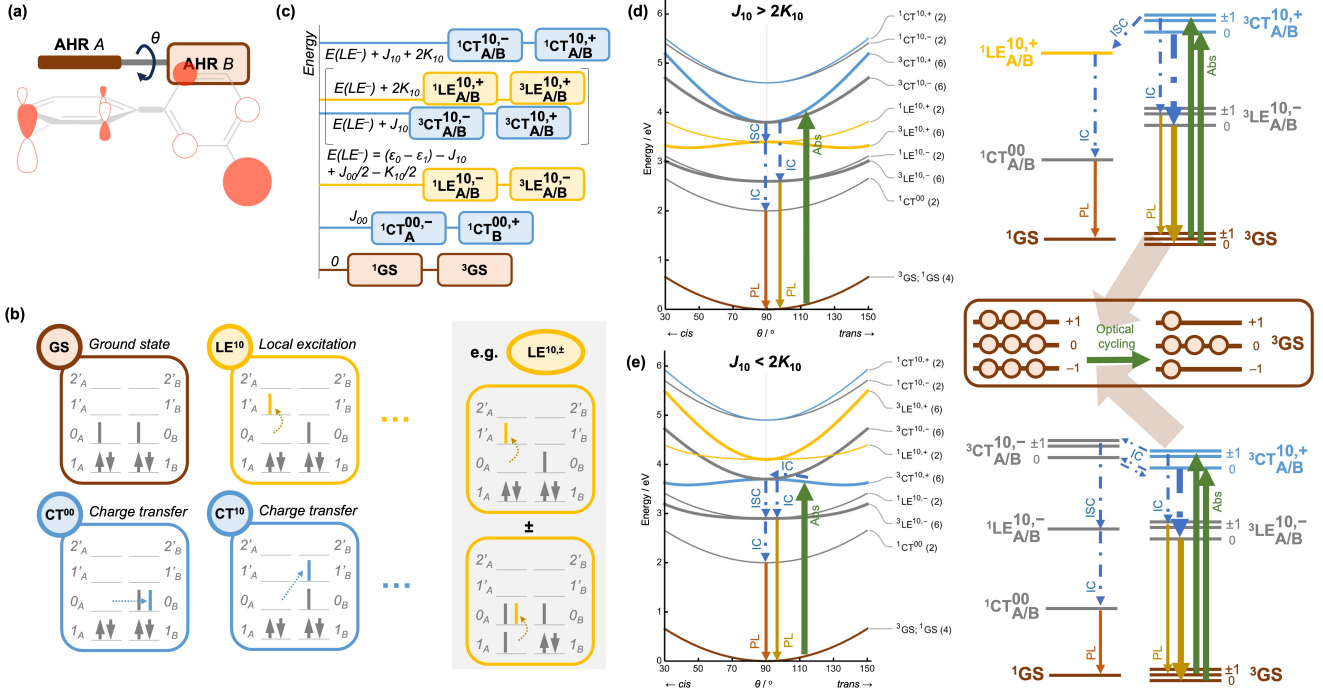


**FIG. 2:** (a) Schematic of an AHR *m*-dimer, which contains two AHRs (indexed  $r \in \{A, B\}$ ) covalently tethered at the unstarred atoms (the class of fewer atoms) with torsional angle  $\theta$ . (b) Ground and excited state configurations of AHR *m*-dimers, expressed in the basis of MOs localised completely on either monomer *A*, i.e.  $\{\dots, 1_A, 0_A, 1'_A, \dots\}$ , or monomer *B*, i.e.  $\{\dots, 1_B, 0_B, 1'_B, \dots\}$ . LEs keep the excited electron on the same monomer (e.g.  $0_A \rightarrow 1'_A$ ), while CTs excite electrons across monomers (e.g.  $0_A \rightarrow 1'_B$ ). Labels “±” represent linear combinations of SOMO-to-LUMO and HOMO-to-SOMO transitions, i.e. particle-hole symmetries. (c) Energies of ground and excited electronic states at  $\hat{V}_{NN} = 0$ , presented in ascending order. The energy ordering between the  $LE^{10,+}$  states and the  $^3CT^{10}$  states depends on the relative values of  $J_{10} \equiv (11|00)$  and  $2K_{10} \equiv 2(10|01)$ . ZFS is not being considered by this work. (d,e) Plots of representative PESs based on perturbation theory calculations for (d)  $J_{10} > 2K_{10}$  and (e)  $J_{10} < 2K_{10}$ . Non-absorptive states are drawn in grey and degeneracies are indicated in parenthesis. Also illustrated are two possible ODMR mechanisms, one for each case. In both cases, spin polarisation is attained in the triplet GS by transferring its  $M_S = \pm 1$  populations into the singlet GS. Parameters for (d):  $E_{\text{steric}} = 0.6$  eV;  $\theta_{\text{eq}} = 90.0^\circ$ ;  $\beta_{AB}^0 = 2.5$  eV;  $\gamma_{AB}^0 = 0$  eV; SOMO-LUMO gap = 3.0 eV;  $c_{A1A} = c_{B1B} = 0.5$ ;  $J_{00} = 2.0$  eV;  $J_{10} = 1.2$  eV;  $K_{10} = 0.4$  eV. Parameters for (e): Same as (d) except  $J_{10} = 0.8$  eV and  $K_{10} = 0.6$  eV. Abs: Photoexcitation.

of these excitations. For simplicity, we consider only the  $1 \rightarrow 0$  and  $0 \rightarrow 1'$  transitions ( $j'$  labels LUMO+ $j$ ), even though the subsequent analysis applies to higher-lying excitations as well (such as  $2 \rightarrow 0$  and  $0 \rightarrow 2'$ ). This totals up to 35 states and their expressions have been compiled in Supplementary Information S2 after taking symmetry- and spin-adapted linear combinations, as described by Eq. (6).

We then compute the zeroth-order excitation energies by taking expectation values over  $\hat{H}_A + \hat{H}_B$ , the results being compiled in Fig. 2c. We highlight that the singlet CT $^P$  state is higher in energy than the triplet ones because, unlike LE $^P$ , the unpaired spins in CT $^P$  experience intramonomer exchange interactions that do not vanish with  $\hat{V}_{AB} \rightarrow 0$ . Also, the  $\{|^1LE_{\Gamma}^{10,+}; 0\}$  and  $\{|^3CT_{\Gamma}^{10,+}; \pm 1\}$  sets may have opposite energy rankings depending on the relative values of  $J_{10} \equiv (11|00)$  and  $2K_{10} \equiv 2(10|01)$  (in chemists’ notation [62]). Finally, while the LE $^+$  and LE $^-$  states are separated in energy due to configuration interaction between the  $1 \rightarrow 0$  and  $0 \rightarrow 1'$  transitions, this separation is not present in the CT states because the two MO transitions, being intermonomer in nature, are non-interacting at  $\hat{V}_{AB} = 0$ . These, as we shall see, are crucial to the ODMR mechanism.

With regard to the linear absorption spectrum, we find that out of all 35 zeroth-order low-lying excitations, only the LE $^+$  states are bright with non-vanishing transition dipole moments. The reason lies in the form of the dipole operator within the neglect of differential overlap assumption invoked

by the PPP model [63]:

$$\hat{\mu} = \sum_{\nu \in \mathcal{N}_A \cup \mathcal{N}_B} \mu_{\nu} \hat{n}_{\nu}, \quad (7)$$

which has “-” particle-hole symmetry and does not excite between monomers. Hence, the GS, being of “-” symmetry, can only be photoexcited locally and to “+” states. (An alternative interpretation is to realise that the  $j \rightarrow 0$  and  $0 \rightarrow j'$  transitions have identical transition dipole moments, so they cancel when taking antisymmetric combinations in Eq. (3) [61, 65].)

Next, we consider perturbative effects on the approximate zeroth-order eigenstates due to  $\hat{V}_{AB}$ . Because  $\hat{V}_{AB}$  is a spin-preserving intermonomer operator of “+” particle-hole symmetry and  $\mathbf{A}$  irrep [Eq. (5)], only CT-type mixing between states of like symmetry can occur:

$$|^{2S+1}LE_{\Gamma}^{10,P}; M_S \rangle \xleftrightarrow{\hat{V}_{AB}} |^{2S+1}CT_{\Gamma}^{10,P}; M_S \rangle. \quad (8)$$

This suggests that CT $^+$  excitations can also be partially bright depending on the extent of LE $^+$  mixing. We note that while  $\hat{V}_{AB}$  can in principle connect GS to CT states and also CT $^{00}$  to LE states, these matrix elements are small because  $\hat{V}_{AB}$  is largest near the dimer linkage where nodes of the SOMOs reside, thus any excitations involving SOMO electrons will be negligible. This is consistent with the notion that, in

AHR  $m$ -dimers,  $\pi$ -bonding – described by mixing of covalent (LE) and ionic (CT) wavefunctions [66] – only occurs in the excited states. Formally, we extend the nearest neighbour approximation to the Coulomb interaction parameter  $\gamma_{\mu\nu}$  (which scales inversely with the distance between  $\mu$  and  $\nu$ ) and expand  $\hat{V}_{AB}$  in terms of MO fermionic operators using  $\hat{a}_{\mu\sigma}^\dagger = \sum_{jr} c_{\mu jr}^* \hat{b}_{jr\sigma}^\dagger$  ( $r$  indexes the monomer containing  $\mu$ ). The result, labelled  $\hat{V}_{NN}$ , reads [Eq. (5)]

$$\begin{aligned} \hat{V}_{AB} &\approx \hat{V}_{NN} \\ &\equiv -\beta_{AB} \sum_{\sigma} \left( \hat{a}_{A\sigma}^\dagger \hat{a}_{B\sigma} + \hat{a}_{B\sigma}^\dagger \hat{a}_{A\sigma} \right) \\ &\quad + \gamma_{AB} \hat{n}_A \hat{n}_B \end{aligned} \quad (9)$$

in the AO basis and

$$\begin{aligned} \hat{V}_{AB} &\approx \hat{V}_{NN} \\ &\equiv -\beta_{AB} \sum_{j_A, k_B} \sum_{\sigma} \left( c_{A j_A}^* c_{B k_B} \hat{b}_{j_A\sigma}^\dagger \hat{b}_{k_B\sigma} \right. \\ &\quad \left. + c_{B k_B}^* c_{A j_A} \hat{b}_{k_B\sigma}^\dagger \hat{b}_{j_A\sigma} \right) \\ &\quad + \gamma_{AB} \sum_{j_A, l_A, k_B, m_B} \sum_{\sigma\tau} c_{A j_A}^* c_{A l_A} c_{B k_B}^* c_{B m_B} \\ &\quad \times \hat{b}_{j_A\sigma}^\dagger \hat{b}_{l_A\sigma} \hat{b}_{k_B\tau}^\dagger \hat{b}_{m_B\tau} \end{aligned} \quad (10)$$

in the MO basis, with  $A$  and  $B$  being the unstarred atoms linking the two AHRs. Because unstarred atoms are where the SOMO's nodes are located, we find that  $c_{A0_A} = c_{B0_B} = 0$ , restricting the sum over  $\{j_A, l_A, k_B, m_B\}$  in Eq. (10) to only non-zero values. This leaves  $\hat{V}_{NN}$  with no excitations connected to the SOMO (index  $j = 0$ ), in line with the above analysis. Importantly, all of these suggest a negligible GS singlet-triplet gap despite  $\hat{V}_{NN} \neq 0$ , a sign of a true diradical.

Corrections to the states and energies are then evaluated to second order in the approximate perturbation  $\hat{V}_{NN}$ , the results being presented in Supplementary Information S3. Importantly, because  $\hat{V}_{NN}$  scales with the degree of  $\pi$ -orbital overlap between the two AHRs, we expect its effects to be quantified by an intermonomer torsional angle  $\theta$  [Fig. 2a] such that the  $\pi$ -interactions are maximal when the two monomers are coplanar at  $\theta = 0^\circ$  or  $180^\circ$ . To this end, we parametrise  $\hat{V}_{NN} = \hat{V}_{NN}(\theta)$  by substituting

$$\beta_{AB} = \beta_{AB}(\theta) \approx \beta_{AB}^0 \cos \theta, \quad (11)$$

$$\gamma_{AB} = \gamma_{AB}(\theta) \approx \gamma_{AB}^0 \cos^2 \theta. \quad (12)$$

Here,  $\cos \theta$  represents the projection of one AHR's local axis of quantisation (the “z-axis”) onto the other's, and two of such terms are necessary for any two-electron integral. An additional parabolic potential is also introduced to model steric effects in the GS:

$$V_{\text{steric}}(\theta) \approx E_{\text{steric}}(\theta - \theta_{\text{eq}})^2, \quad (13)$$

which we assume to be the same in the excited states. In general, we expect  $\theta_{\text{eq}} \approx 90^\circ$  due to the lack of  $\pi$ -bonding in the GS.

Based on the perturbation theory results and the above  $\theta$  parametrisation, we plotted two representative potential energy surfaces (PESs) in Fig. 2d,e. Indeed, the singlet and triplet GSs are degenerate over the entire range of  $\theta$ , consistent with the lack of radical-radical interactions in the GS. The same holds for LE states at  $\theta = 90^\circ$  (because  $\hat{V}_{AB} = 0$ ). However, away from this angle, mixing with the CT states opens up a gap between the two spin multiplicities – a sign of  $\pi$ -bonding [66].

The ODMR cycle is only complete with a spin-selective ISC, the key towards spin polarisation. At the heart of this

effect is the SOC operator that controls the ISC rate and, as mentioned earlier, only links rotated  $\pi$ -orbitals [51–54]. Because AHRs are mostly planar, SOC will have to be an intermonomer effect that is largest at the maximum torsion of  $\theta = 90^\circ$ . Furthermore, we expect this operator to act locally at the dimer connection since its matrix elements scale inversely with the cube of the interatomic distance. Given these restrictions, we further examine the nature of SOC by adapting the single-electron Breit-Pauli SOC operator in PPP theory [53] to our system. We obtain

$$\hat{V}_{\text{SOC}}(\theta) = \sum_{\sigma} B \sin(\theta) \left( \hat{a}_{A\sigma}^\dagger \hat{a}_{B\bar{\sigma}} - \hat{a}_{B\bar{\sigma}}^\dagger \hat{a}_{A\sigma} \right), \quad (14)$$

or, in terms of MO operators,

$$\begin{aligned} \hat{V}_{\text{SOC}}(\theta) &= \sum_{j_A \neq 0_A, k_B \neq 0_B} \sum_{\sigma} B \sin(\theta) \left( c_{A j_A}^* c_{B k_B} \hat{b}_{j_A\sigma}^\dagger \hat{b}_{k_B\bar{\sigma}} \right. \\ &\quad \left. - c_{B k_B}^* c_{A j_A} \hat{b}_{k_B\bar{\sigma}}^\dagger \hat{b}_{j_A\sigma} \right), \end{aligned} \quad (15)$$

where  $B$  is a purely imaginary value defined in Supplementary Information S4. Similar to the analysis of  $\hat{V}_{AB}$ , we find that  $\hat{V}_{\text{SOC}}$  only couples LE and CT excitations and leaves the GS and  $\text{CT}^{00}$  states unperturbed due to the SOMO's nodal structure. It creates spin flips, has “+” particle-hole symmetry and is odd under  $C_2$  rotation. Hence, we find that the only allowed ISC processes are

$$|^1\text{LE}_{\Gamma}^{10,P}; 0\rangle \xleftrightarrow{\hat{V}_{\text{SOC}}} |^3\text{CT}_{\bar{\Gamma}}^{10,P}; \pm 1\rangle, \quad (16)$$

$$|^3\text{LE}_{\Gamma}^{10,P}; \pm 1\rangle \xleftrightarrow{\hat{V}_{\text{SOC}}} |^1\text{CT}_{\bar{\Gamma}}^{10,P}; 0\rangle, \quad (17)$$

with  $\bar{\Gamma}$  being the irrep opposite to  $\Gamma$ . As an aside, in deriving Eq. (15) we have assumed the dimer linkage to be perpendicular to the spin quantisation axis (Supplementary Note S4). When no magnetic field is applied, the latter is determined by the spin-spin interactions intrinsic to the molecule [67]. This implies spin quantisation along the high-symmetry axis of the molecule, making the earlier assumption valid in AHR  $m$ -dimers given the orientation of the  $C_2$  axis.

## B. Proposed ODMR mechanisms

To sum it up, a detailed electronic structure analysis of AHR  $m$ -dimers revealed important symmetries that affect the ODMR mechanism. Of particular importance are the following:

- Excited states may be classified based on their character at torsion  $\theta = 90^\circ$  [Fig. 2a]. This can be either local excitations (LEs), which promote electrons in an intramonomer fashion, or charge transfers (CTs), which move electrons across monomers [Fig. 2b]. Also labelled are the state's particle-hole symmetry (a consequence of alternacy symmetry), which can be either “+” or “-” [Eq. (6)]. These states are ordered by energy in Fig. 2c. (Aside: States are also labelled by their irrep  $\Gamma \in \{\text{A}, \text{B}\}$ , but this is inconsequential to the ODMR mechanism.)
- Near the equilibrium torsion of  $\theta \approx 90^\circ$  [Fig. 2a], intermonomer  $\pi$ -bonding is negligible. Therefore, only the CT states have appreciable singlet-triplet gaps due to intramonomer exchange interactions [Fig. 2c]. This implies that selective photoexcitation of the triplets (over the singlets) can only occur to CT-dominated states.

- c. Of all lowest-lying LE and CT excitations, only LE states of “+” particle-hole symmetry are bright at  $\theta = 90^\circ$  [Eq. (7)]. However, CT states of “+” particle-hole symmetry can borrow intensity from these LE states at  $\theta$  values away from  $90^\circ$  due to intermonomer  $\pi$ -bonding [Eqs. (10), (11) and (12)].
- d. ISC is fastest at  $\theta = 90^\circ$ , between CT and LE states, between states of like particle-hole symmetry, and when the triplet  $M_S = \pm 1$  levels are involved – this aligns with El-Sayed rules [50]. In addition, ISC processes involving the  $|^1\text{CT}^{00,-}\rangle$  and  $|^1\text{CT}^{00,+}\rangle$  states are slow because the SOMO has a node at the bond connecting the two monomers [Eqs. (15), (16) and (17)].

These observations are consistent with those made in the introduction. From here, we report two possible pathways for ODMR according to the excitation energies [Fig. 2c]:

1. In the first case where  $J_{10} > 2K_{10}$  [Fig. 2d], we propose to directly photoexcite the  $|^3\text{CT}^{10,+}\rangle$  states at  $\theta$  values away from  $90^\circ$  (via thermal effects) where mixing with the  $|^3\text{LE}^{10,+}\rangle$  states is appreciable. Relaxation to the equilibrium torsion of  $\theta \approx 90^\circ$  is expected. At this point, ISC effects are strongest and couple the  $M_S = \pm 1$  sublevels of the  $|^3\text{CT}^{10,+}\rangle$  state to the  $|^1\text{LE}^{10,+}\rangle$  state, selectively depopulating the triplet  $M_S = \pm 1$  levels. Following Kasha’s rule, the resulting  $|^1\text{LE}^{10,+}\rangle$  population should emit from the  $|^1\text{CT}^{00,-}\rangle$  and  $|^1\text{CT}^{00,+}\rangle$  states, relaxing to the ground singlet state. As for the remaining  $|^3\text{CT}^{10,+}\rangle$  molecules in the  $M_S = 0$  level, emission to the ground triplet state should occur through the  $|^3\text{LE}^{10,-}\rangle$  states ( $M_S = 0$ ) at a different wavelength from the singlets, offering optical readout of the triplet  $M_S = 0$  levels. We note that both non-radiative internal conversions (ICs) and emissions are spin-preserving. Therefore, overall, population from the triplet  $M_S = \pm 1$  ground levels have been transferred away to the singlet ground state, creating ground state spin polarisation. Since ISC rates decay exponentially with the energy gap [68], this mechanism works best when the  $|^3\text{CT}^{10,+}\rangle$  and  $|^1\text{LE}^{10,+}\rangle$  states lie close in energy, achieved when  $J_{10} \approx 2K_{10}$ .
2. In the second case where  $J_{10} < 2K_{10}$  [Fig. 2e], the photoexcited  $|^3\text{CT}^{10,+}\rangle$  molecules can, through a single-phonon process, rotate to  $\theta \approx 90^\circ$ , at which point the  $|^3\text{CT}^{10,-}\rangle$  states are near-degenerate and directly accessible via spin-preserving ICs [68]. This is also the geometry with the best ISC, taking  $|^3\text{CT}^{10,-}\rangle$  to  $|^1\text{LE}^{10,-}\rangle$  through the triplet  $M_S = \pm 1$  sublevels, which then relaxes to the ground singlet state. Meanwhile, the remaining triplet  $M_S = 0$  population in the  $|^3\text{CT}^{10}\rangle$  states have no ISC channel and will return to the ground triplet state, with optical readout being possible because emissions from both spin multiplicities are distinguishable by wavelength (just like in case 1). This mechanism works best with smaller  $J_{10}$  values because not only is the rotation barrier on the  $|^3\text{CT}^{10,+}\rangle$  surfaces smaller, but also ISC can occur over a smaller energy gap.

A few points are now in order: Firstly, photoexcitation away from the equilibrium torsion of  $\theta \approx 90^\circ$  is possible at room temperature, verified by ab initio calculations (more to follow) and with the trade-off of faster spin decoherence. Next, while the  $|^1\text{GS}\rangle \rightarrow |^3\text{GS}\rangle$  ISC through the triplet  $M_S = \pm 1$  sublevels will lead to spin relaxation, such couplings are not mediated by the single-electron Breit-Pauli SOC due to the operator’s CT nature [Eq. (15)]. Thirdly, while LE<sup>−</sup> and CT states of AHR dimers are, at  $\theta \approx 90^\circ$  torsion, less emissive than their LE<sup>+</sup> counterparts [Eq. (7)], PL can still be

detected; for instance, TTM radicals have quantum yields of around 0.02 with emission from LE<sup>−</sup> states [39, 65, 69]. On a related note, we did not explicitly model IC in the PPP framework but only expected them to occur without preserving particle-hole symmetry, as with most AHRs [61, 65]. Finally, because spins are polarised by shelving triplet  $M_S = \pm 1$  population into the singlet state, at most 25% of the ensemble will be a triplet  $M_S = 0$ , unlike the NV centre where this value is 100%.

Note that even though we have described only the  $1 \rightarrow 0$  and  $0 \rightarrow 1'$  excitations for simplicity, the same selection rules apply to any general  $j \rightarrow 0$  and  $0 \rightarrow j'$  transitions ( $j > 0$ ), which may be low-lying in some AHR  $m$ -dimers.

### C. Validation by ab initio calculations

To set the results in the context of existing systems, we consider two specific AHRs: A methylated benzylic radical [Fig. 3a] and TTM [Fig. 4a]. Ground-state properties of the AHR  $m$ -dimers were calculated using unrestricted DFT at the B3LYP/6-31G(d,p) level. In both cases, significant torsion was found at the equilibrium geometry, with  $\theta_{\text{eq}}$  values of  $91.9^\circ$  and  $92.9^\circ$  respectively. Through calculations converging to the open-shell broken-symmetry (BS) state, we also found small singlet-triplet energy gaps ( $\Delta E_{\text{ST}}$ ) at both  $\theta = 90^\circ$  ( $-0.003$  eV and  $-0.053$  eV respectively) and  $\theta = 110^\circ$  ( $-0.006$  eV and  $-0.031$  eV), indicating weak exchange interactions between the two monoradicals [70]. Indeed, the two SOMOs of the BS state were degenerate, each localised on separate monomers [Fig. 3,4b]. Closed-shell singlet (CS) states were also found, with energies that were at least 1.0 eV higher than the open-shell triplet states (respective values: 1.021 eV and 1.031 eV at  $\theta = 90^\circ$ ; 0.974 eV and 1.019 eV at  $\theta = 110^\circ$ ). This suggests that AHR  $m$ -dimers are likely to be open-shell diradicals in the ground state across different torsional angles  $\theta$ . Finally, rotating the molecules away from  $\theta = 90^\circ$  distributed the HOMOs and LUMOs (but not the SOMOs) of the BS state across the dimer, a sign of interradical interactions in the excited states [Fig. 3,4b]. These findings are consistent with the analytical results from the PPP Hamiltonian.

For the methylated benzylic radical  $m$ -dimer, multi-configurational self-consistent field (MCSCF) and configuration interaction (CI) methods were also used to verify the DFT calculations.  $\Delta E_{\text{ST}}$  was computed to be  $-0.004$  eV at  $\theta = 90^\circ$  and  $-0.009$  eV at  $\theta = 110^\circ$  with the first excited singlet energies being 2.227 eV and 2.207 eV respectively relative to the triplet ground state. These results agree with those from ground-state DFT (note that the CS energy is approximately half of the first singlet excitation energy; see Methods).

We also approximated the width of the Boltzmann distribution of  $\theta$  by  $\Delta\theta \equiv \sqrt{k_B T / E_{\text{steric}}}$  [Eq. (13)] with  $k_B$  and  $T$  representing the Boltzmann constant and temperature respectively. For both AHR  $m$ -dimers,  $\Delta\theta = 12^\circ$  at  $T = 298$  K, indicating that excitation away from  $\theta = 90^\circ$ , required for ODMR [Fig. 2d,e], may be achieved by operating at room temperature (at the expense of enhancing deleterious decoherence processes). Importantly, this value can be tuned by modifying the degree of steric hindrance at the dimer linkage. As an example, to the methylated benzylic radical  $m$ -dimer, we removed the methyl substituents closest to the dimer linkage that are *ortho* to the methylene group. This widened the ground-state PES, yielding the same  $\Delta\theta$  value at a lower temperature of  $T = 108$  K (Supplementary Information S7).

Coulomb and exchange integrals among the MOs were then estimated from the excited-state properties of the monoradicals using unrestricted time-dependent DFT (TD-DFT) calculations, conducted within the Tamm–Dancoff ap-

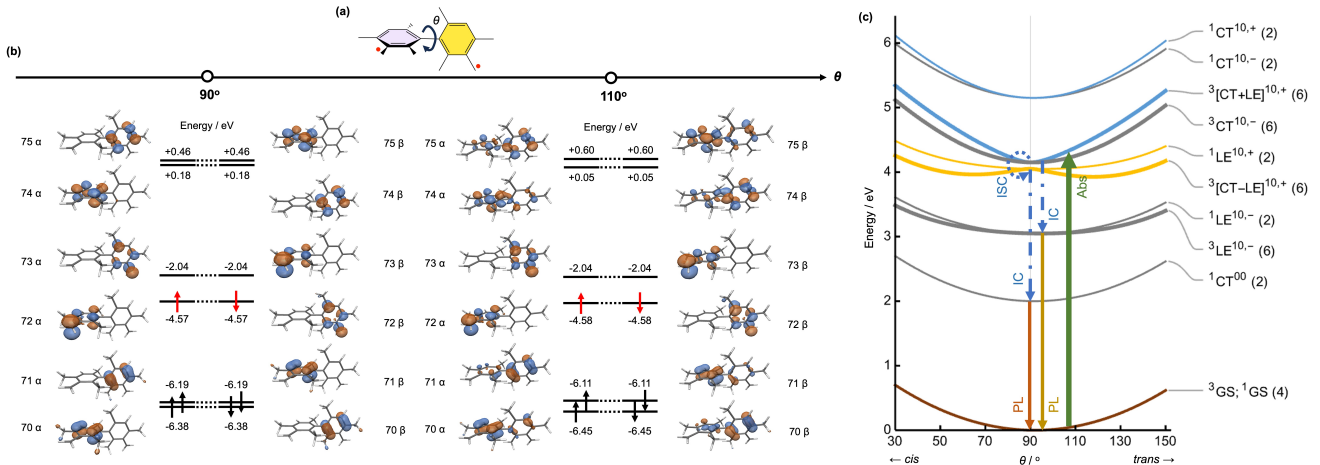


**FIG. 3:** (a) Structure of an AHR *m*-dimer constructed using two methylated benzylic radicals. (b) Frontier MOs (isovalue = 0.060) of the dimer in the open-shell BS ground state at two different conformations ( $\theta = 90^\circ$  and  $110^\circ$ ), calculated using DFT (UB3LYP/6-31G(d,p)). (c) Plots of PESs using parameters from a TDDFT/TDA calculation (UB3LYP/6-31G(d,p)) of the monoradical. Parameters:  $E_{\text{steric}} = 0.6$  eV;  $\theta_{\text{eq}} = 91.9^\circ$ ;  $\beta_{\mathcal{A}\mathcal{B}}^0 = 2.5$  eV;  $\gamma_{\mathcal{A}\mathcal{B}}^0 = 0$  eV; SOMO-LUMO gap = 3.4 eV;  $c_{\mathcal{A}1_A} = c_{\mathcal{B}1_B} = 0.5$ ;  $J_{00} = 2.0$  eV;  $J_{10} = 1.1$  eV;  $K_{10} = 0.5$  eV.

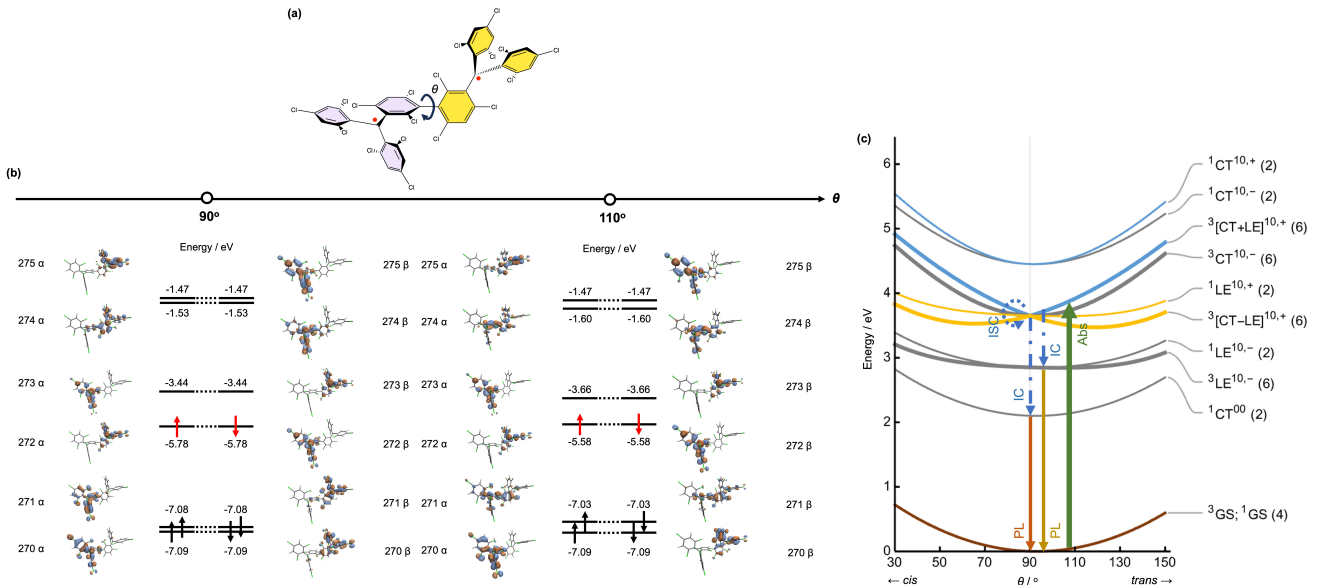


**FIG. 4:** (a) Structure of an AHR *m*-dimer constructed using two TTM radicals. (b) Frontier MOs (isovalue = 0.030) of the dimer in the open-shell BS ground state at two different conformations ( $\theta = 90^\circ$  and  $110^\circ$ ), calculated using DFT (UB3LYP/6-31G(d,p)). (c) Plots of PESs using parameters from a TDDFT/TDA calculation (UB3LYP/6-31G(d,p)) of the monoradical. Parameters:  $E_{\text{steric}} = 0.6$  eV;  $\theta_{\text{eq}} = 92.9^\circ$ ;  $\beta_{\mathcal{A}\mathcal{B}}^0 = 2.5$  eV;  $\gamma_{\mathcal{A}\mathcal{B}}^0 = 0$  eV; SOMO-LUMO gap = 2.8 eV;  $c_{\mathcal{A}1_A} = c_{\mathcal{B}1_B} = 0.5$ ;  $J_{00} = 2.1$  eV;  $J_{10} = 0.8$  eV;  $K_{10} = 0.4$  eV.

proximation (TDA) and with the same functional and basis set as the dimers. We note that these excitation energies have poorer accuracies of  $\sim 0.3$  eV than a rigorous multi-reference electron correlation approach [71] but are nevertheless sufficient for the present goal of setting our analytical results in the correct parameter range. With the methylated benzylic radical, an additional  $|\Psi_{02}; \pm 1/2\rangle$  state (following the notation of Eq. (3)) was found to lie between the  $|\Psi_{01}^-; \pm 1/2\rangle$  and  $|\Psi_{01}^+; \pm 1/2\rangle$  excitations. Because states of “ $-$ ” particle-hole symmetry are dark, the  $|\Psi_{02}^-; \pm 1/2\rangle$  excitation only contributes an additional intermediate state for non-radiative decay and does not affect the overall ODMR process. Other than that, the methylated benzylic radical is an example of case 1, with  $J_{10} \approx 1.1$  eV and  $K_{10} \approx 0.5$  eV. We note that given the small energy dif-

ference between  $J_{10}$  and  $2K_{10}$ , perturbation theory in  $\hat{V}_{\text{NN}}$  between the  $|{}^3\text{LE}_{\Gamma}^{10,+}; M_S\rangle$  and  $|{}^3\text{CT}_{\Gamma}^{10,+}; M_S\rangle$  states breaks down and it is necessary to exactly diagonalise the matrix representation of  $\hat{V}_{\text{NN}}$  within this subspace; these eigenstates are labelled  $|{}^3[\text{CT} \pm \text{LE}]_{\Gamma}^{10,+}; M_S\rangle$  (see Supplementary Information S5). Despite that, the ODMR mechanism remains unchanged [Fig. 3c].

A smaller  $J_{10}$  value is desirable for case 1 because the energy gap for ISC will be reduced. This may be achieved by extending the degree of  $\pi$ -conjugation, which spreads the electron clouds of the valence MOs out, thereby reducing Coulombic repulsion between the occupying electrons. Indeed, the TTM radical, which has a (chlorinated) benzylic radical  $\pi$ -conjugated to two more (chlorinated) phenyl groups, was estimated to have a lower  $J_{10}$  value of  $\approx 0.8$  eV

$(K_{10} \approx 0.4 \text{ eV})$  when averaged over its five near-degenerate lowest energy LUMOs. This places the TTM  $m$ -dimer in the most ideal scenario for case 1 of ODMR in AHR  $m$ -dimers [Fig. 4c].

Because the MCSCF/CI approach fully describes the multi-configurational nature of the methylated benzylic radical  $m$ -dimer, we used that to verify the PPP model parameters, which we had obtained earlier from a single-reference TDDFT/TDA calculation of the monoradical. At this level of theory, we estimated SOMO-LUMO gap  $\approx 3.4 \text{ eV}$ ,  $J_{00} \approx 2.2 \text{ eV}$ ,  $J_{10} \approx 1.0 \text{ eV}$ , and  $K_{10} \approx 0.6 \text{ eV}$ . PESs plotted using these parameters agree well with the MCSCF/CI calculations [Fig. 5a,b]. By placing  $J_{10}$  and  $2K_{10}$  at slightly different values from TDDFT/TDA (with differences of  $\approx 0.1 \text{ eV}$ ), MCSCF/CI changed the ODMR mechanism to that of case 2 [Fig. 5b]. Nevertheless, we believe both mechanisms to be possible given the uncertainty in TDDFT/TDA energies and the sensitivity of MCSCF/CI results to input parameters. Another advantage of the MCSCF/CI method is the possibility for ab initio SOC calculations. Indeed, only CT-type ISCs had appreciable SOC matrix elements with  $\Delta M_S = \pm 1$  selectivity, in agreement with Eqs. (16) and (17) (Supplementary Information S7). All these lend credence to the semiempirical analysis described earlier.

#### D. Mapping the triplet ground state to a controllable qubit

Finally, we note that the triplet ground state of AHR  $m$ -dimers is likely to have minimal zero-field splittings (ZFSs) due to weak spin dipolar interactions between spatially separated radicals [67]. As such, a two-state qubit cannot be isolated by simply applying an external magnetic field, in contrast to the diamond-NV centre. Nevertheless, we propose for an *effective* qubit with the  $M_S = 0$  sublevel being one of the qubit states and the  $M_S = \pm 1$  sublevels functioning collectively as an *effective* second qubit state. This is possible because for systems of two non-interacting electron spins experiencing an external magnetic field along its quantisation axis ( $C_2$  axis for AHR  $m$ -dimers), circularly-polarised microwave light will produce unitary operations of the 3D rotation group SO(3), that is, it rotates the  $|M_S = 0\rangle$  or  $|z\rangle$  state into linear combinations of  $|x\rangle$  and  $|y\rangle$  states, defined as

$$|x\rangle \equiv \frac{|M_S = +1\rangle - |M_S = -1\rangle}{\sqrt{2}}, \quad (18)$$

$$|y\rangle \equiv i \frac{|M_S = +1\rangle + |M_S = -1\rangle}{\sqrt{2}}. \quad (19)$$

For instance, if an AHR  $m$ -dimer were to be spin polarised into an initial quantum state of  $|\psi\rangle = |z\rangle$ , then a microwave pulse will drive it into

$$|\psi\rangle \rightarrow |\psi'\rangle = a|x\rangle + b|y\rangle + c|z\rangle, \quad (20)$$

keeping  $a, b, c \in \mathbb{R}$  and preserving the norm of  $a^2 + b^2 + c^2 = 1$ . In spherical coordinates, this reads

$$|\psi'\rangle = \sin \theta \cos \phi |x\rangle + \sin \theta \sin \phi |y\rangle + \cos \theta |z\rangle, \quad (21)$$

with  $\theta \in [0, \pi]$  and  $\phi \in [0, 2\pi]$ . Since two real numbers are sufficient to describe a qubit state, an effective qubit arises here because the normalised state  $|\psi'\rangle$  is also characterised by two real-valued coefficients  $\theta$  and  $\phi$ . In this way, the  $M_S = \pm 1$  sublevels have become the second qubit state through either  $|x\rangle$  or  $|y\rangle$  (with the other state being redundant). This is essentially a statement of the isomorphism between SO(3) and SU(2), the latter of which describes a

qubit. Here, our accessible pure state space is a unit 2-sphere with the three Cartesian axes corresponding to  $|x\rangle$ ,  $|y\rangle$  and  $|z\rangle$  states, analogous to the Bloch sphere for a pure qubit state [Table 1].

To see how circularly-polarised microwave pulses result in unitary operations of the SO(3) group, we consider a Hamiltonian  $\mathcal{H}$  of two electron spins  $\hat{S}_j$  ( $j \in \{A, B\}$ ) with negligible exchange and spin-dipolar couplings. Both spins are precessing under the influence of both a static magnetic field  $B_0 \mathbf{z}$  and an oscillating circularly-polarised microwave field  $B_1 [\cos(\omega t) \mathbf{x} + \sin(\omega t) \mathbf{y}]$  ( $\mathbf{x}$ ,  $\mathbf{y}$  and  $\mathbf{z}$  are unit vectors of the Cartesian axes). This Hamiltonian reads

$$\mathcal{H}(t) = \sum_{j=A,B} g_j \mu_B \left[ B_0 \hat{S}_{j,z} + B_1 \hat{S}_{j,x} \cos(\omega t) + B_1 \hat{S}_{j,y} \sin(\omega t) \right], \quad (22)$$

where  $g_j$  is the  $g$ -factor of electron  $j$  and  $\mu_B$  is the Bohr magneton. By substituting  $g_A = g_B \equiv g$  for dimers and  $\hat{\mathbf{S}} \equiv \hat{\mathbf{S}}_A + \hat{\mathbf{S}}_B$  as the total spin operator, we find  $\mathcal{H}$  in the rotating frame of the oscillating field to be

$$\mathcal{H}_{\text{r.f.}} = (g\mu_B B_0 - \hbar\omega) \hat{S}_z + g\mu_B B_1 \hat{S}_x. \quad (23)$$

Thus, the time evolution operator at resonance is  $\hat{U}(t) = \exp(-i\omega_1 \hat{S}_x t)$ , the rotation operator about the  $x$ -axis by angle  $\omega_1 t$  ( $\omega_1 \equiv g\mu_B B_1/\hbar$ ). Similarly, a  $y$ -axis rotation may be obtained by shining light of the opposite polarisation. Thus, through a series of microwave pulses we can achieve any arbitrary single qubit operation in our effective qubit (for instance, through the  $X$ - $Y$  decomposition [72]), satisfying the generality criteria.

We note that general rotations of a three-level system (qutrit) belong to the SU(3) group, which contains the SO(3) group, so the operations proposed above are only a subset of all possible rotations in a qutrit, an observation consistent with our mapping of a qutrit to a qubit.

### III. CONCLUSION

In conclusion, we demonstrate AHR  $m$ -dimers to be promising sources of fully-organic molecular colour centres. By analysing their electronic structure using the PPP framework, we propose different ODMR mechanisms for different energetic orderings of the excited states. The general principle is the same in all cases: Because the SOC operator, responsible for spin filtering through its  $\Delta M_S = \pm 1$  rule, only mediates transitions across two rotated AHRs, charge transfer must be engineered between a triplet and a singlet in the excited states. Moreover, only CT-type excited states have energetically well-separated singlet and triplet levels because an unpaired electron from one monoradical has been excited into the other monomer and thus experiences stronger exchange interactions. Therefore, one may begin with a CT-type photoexcitation of *only* the triplet molecules, which will then see their  $M_S = \pm 1$  population reverse the charge transfer, via SOC, to the singlet excited states, i.e. undergo spin-selective ISC. The excited-state spin polarisation may then be transferred to the ground state via any series of spin-selective relaxation, such as IC or emission. Since the emission probabilities and wavelengths of the triplet  $M_S$  levels will be different due to different decay channels ( $\pm 1$  through the singlets and 0 through the triplets), one can achieve optical readout of the ground-state spin polarisation by observing changes to the emission spectrum. The specific method for optical readout will differ based on the molecular parameters.

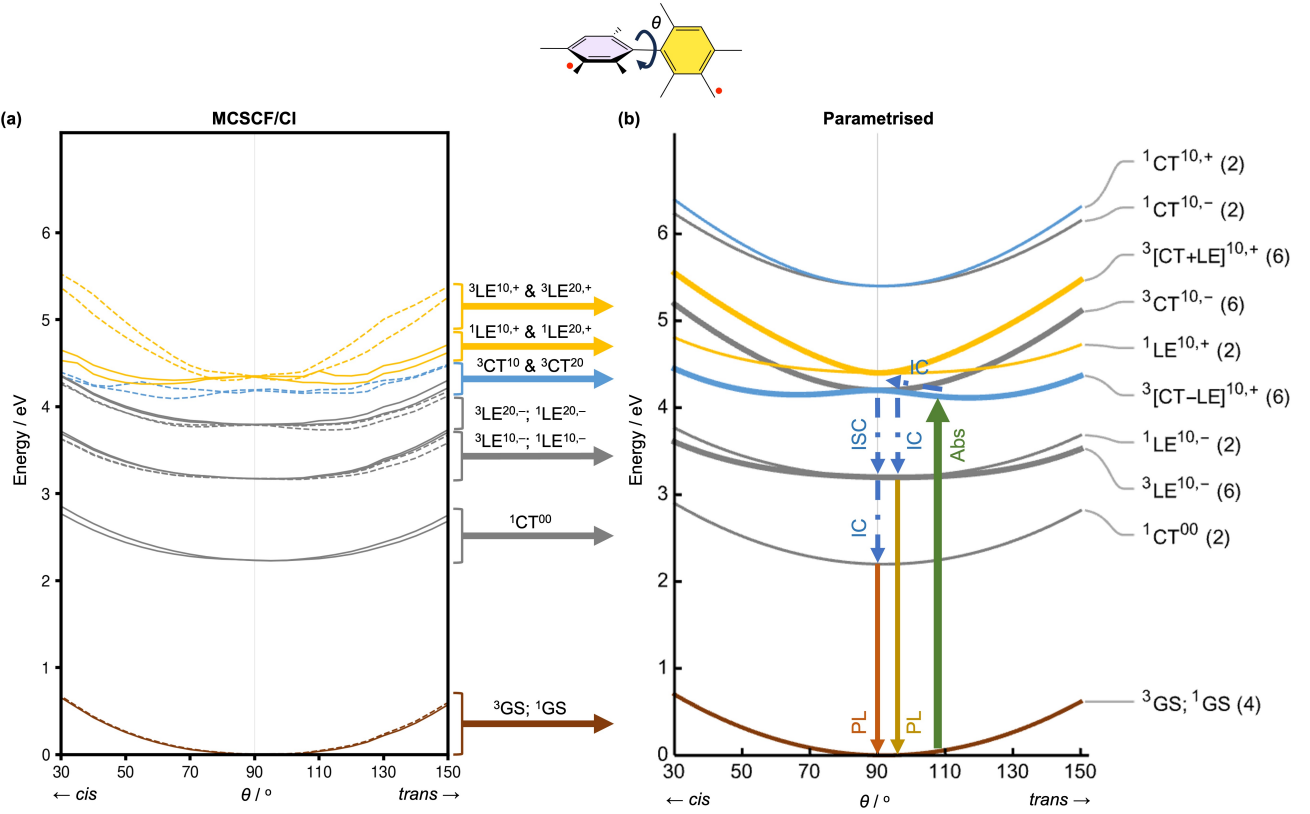


**FIG. 5:** (a) PESs of the nine lowest-lying triplet  $M_S = +1$  states (dashed lines) and the nine lowest-lying singlet states (solid lines) of the methylated benzyl radical  $m$ -dimer, obtained with MCSCF/CI/6-31G(d,p) calculations. States were assigned based on their characters at  $\theta \approx 90^\circ$ . (b) Plots of PESs using parameters from MCSCF/CI/6-31G(d,p) calculations of the  $m$ -dimer. Parameters:  $E_{\text{steric}} = 0.6 \text{ eV}$ ;  $\theta_{\text{eq}} = 91.9^\circ$ ;  $\beta_{AB}^0 = 2.5 \text{ eV}$ ;  $\gamma_{AB}^0 = 0 \text{ eV}$ ; SOMO-LUMO gap = 3.4 eV;  $c_{A1A} = c_{B1B} = 0.5$ ;  $J_{00} = 2.2 \text{ eV}$ ;  $J_{10} = 1.0 \text{ eV}$ ;  $K_{10} = 0.6 \text{ eV}$ .

**TABLE 1:** Mapping between a standard qubit and our effective qubit. A pure qubit state “lives” on a Bloch sphere spanned by eigenstates of the Pauli vector operator  $\hat{\sigma}$ , denoted here by  $\{| \uparrow \rangle, | \downarrow \rangle\}$ . The general form of a single qubit operator is thus a rotation on the Bloch sphere, generated by  $\mathbf{n} \cdot \hat{\sigma}/2$  for some unit vector  $\mathbf{n}$ . Because our effective qubit state, if pure, can only access a unit sphere in 3D real space, the corresponding single qubit operator is a 3D rotation, generated by  $\mathbf{n} \cdot \hat{\mathbf{S}}$ . Here,  $\hat{\mathbf{S}}$  is the spin-1 operator with eigenstates  $\{|M_S\rangle |M_S = -1, 0, +1\}$ , where  $|z\rangle \equiv |M_S = 0\rangle$  and  $\{|x\rangle, |y\rangle\}$  are linear combinations of  $\{|M_S = \pm 1\rangle\}$  states [Eqs. (18) and (19)].

	Standard qubit	Our effective qubit
Pure state	$ \psi\rangle = \cos(\theta/2) \uparrow\rangle + e^{i\phi}\sin(\theta/2) \downarrow\rangle$ with $\theta \in [0, \pi]$ and $\phi \in [0, 2\pi]$	$ \psi\rangle = \sin\theta\cos\phi x\rangle + \sin\theta\sin\phi y\rangle + \cos\theta z\rangle$ with $\theta \in [0, \pi]$ and $\phi \in [0, 2\pi]$
Single qubit operator	$\hat{R}_{\mathbf{n}}(\theta) = e^{-i\theta\mathbf{n} \cdot \hat{\sigma}/2}$	$\hat{R}_{\mathbf{n}}(\theta) = e^{-i\theta\mathbf{n} \cdot \hat{\mathbf{S}}}$

To the best of our knowledge, this is the first theoretical analysis on carbon-based optically-addressable molecular qubits and we hope that our findings can guide future efforts in this field. To this end, we have outlined the possibility of driving the ZFS-free triplet sublevels using microwave pulses, an example of a single qubit operation. Ongoing efforts include further structural optimisation of AHR  $m$ -dimers and generalisation of the qubit pulse protocol using a density matrix formalism.

#### IV. METHODS

Unless otherwise stated, all DFT-based calculations were performed using the Q-Chem package (version 6.0.2) [73]. In the next two paragraphs, we describe our DFT methods,

conducted at the UB3LYP/6-31G(d,p) level and in vacuo. Ground-state geometries of the AHR  $m$ -dimers were optimised as triplets and PES scans were performed as triplets over  $20^\circ \leq \theta \leq 160^\circ$  (interval =  $5^\circ$ ), of which the resulting energies were fitted into  $V_{\text{steric}}$  [Eq. (13)]. Using geometries obtained for  $\theta = 90^\circ$  and  $110^\circ$  (*trans*), energies of the open-shell singlet were found by the spin-unrestricted BS approach and used to compute  $\Delta E_{\text{ST}}$  following Yamaguchi et al. [74]:

$$\Delta E_{\text{ST}} \equiv E_{\text{S}} - E_{\text{T}} = \frac{\langle \mathbf{S}^2 \rangle_{\text{T}}}{\langle \mathbf{S}^2 \rangle_{\text{T}} - \langle \mathbf{S}^2 \rangle_{\text{BS}}} (E_{\text{BS}} - E_{\text{T}}). \quad (1)$$

Energies of the CS states were also computed at the same conformations. Due to  $C_2$  symmetry, the CS states were described by  $|\cdots 1_+ \overline{1}_+ 1_- \overline{1}_- 0_+ \overline{0}_+\rangle$  with  $j_{\pm} \approx 2^{-1/2} (j_A \pm j_B)$  ( $j = \cdots, 1, 0, 1', \cdots$ ). Hence, for AHR  $m$ -dimers described

by the PPP Hamiltonian  $\hat{H}$  [Eqs. (4) and (5)], the CS states will have energies of

$$E_{\text{CS}} \approx E_{\text{T}} + \frac{J_{00}}{2} \quad (2)$$

(Supplementary Information S6). From that, we estimated the values of  $J_{00}$ .

Geometries of AHR monomers were optimised as doublets, following which unrestricted TDDFT/TDA was applied without further structural changes. For the methylated benzylic radical, the SOMO-LUMO gap ( $\varepsilon_{01}$ ) was estimated as half of the HOMO-LUMO gap. Within the mean-field approach set by Longuet-Higgins and Pople [58–60], we find  $J_{10}$  and  $K_{10}$  to have the following expressions:

$$K_{10} = \frac{E_{01}^+ - E_{01}^-}{2}, \quad (3)$$

$$J_{10} = -E_{01}^- + \varepsilon_{01} + \frac{J_{00}}{2} - \frac{1}{2}K_{10}, \quad (4)$$

where  $E_{01}^\pm$  are the excitation energies of  $|\Psi_{01}^\pm; +1/2\rangle$ , estimated using TDDFT/TDA. A similar approach was taken for the TTM radical. However, because the highest-energy HOMOs and lowest-energy LUMOs were (almost) five-fold degenerate each, for simplicity the  $\{(j \rightarrow 0) | 1 \leq j \leq 5\}$  and  $\{(0 \rightarrow j') | 1 \leq j \leq 5\}$  sets of lowest-lying excitations were each modelled as effective single  $1 \rightarrow 0$  and  $0 \rightarrow 1'$  excitations with parameters averaged over the five MOs. This is sufficient to place the PPP model parameters in the correct energy range.

For the methylated benzylic radical *m*-dimer, MCSCF calculations were performed on the UB3LYP-optimised triplet ground-state geometry using the complete active space self-consistent field (CASSCF) method. We conducted state-specific CASSCF(10,10) calculations to obtain the ground triplet and singlet states, following which the excited states were estimated using the complete active space configuration interaction (CASCI) method. All states and energies were corrected by the van Vleck quasi-degenerate

(QD) extension to the strongly contracted second-order N-electron valence state perturbation theory (SC-NEVPT2). We were able to classify all lowest-lying excited states into an excitation from Fig. 2c by observing the CI vector characters and oscillator strengths. This allowed us to estimate the parameters  $\varepsilon_{01}$ ,  $J_{00}$ ,  $J_{10}$ , and  $K_{10}$  by comparing the computed energies with the expressions in Fig. 2c. In particular, the first singlet excitation had  $\text{CT}^{00}$  character, placing its energy at approximately  $J_{00}$  or twice that of the DFT CS state [Eq. (2)]. Meanwhile, SOC matrix elements were computed between singlet and triplet wavefunctions of a CASCI/QD-SC-NEVPT2 calculation using state-specific orbitals optimised by CASSCF(10,10) for the triplet ground state. Only for this calculation were the orbitals shared between singlets and triplets. Also, the  $\hat{S}_z$  eigenbasis was used to express the electron spin states with the  $z$ -axis aligned to the molecular  $C_2$  axis – these are the most-likely spin eigenstates of the molecule (see discussion following Eq. (17)). Finally, ground and excited PESs were estimated via the same state-specific CASSCF(10,10)/CASCI/QD-SC-NEVPT2 strategy with separate orbitals for singlets and triplets and using the UB3LYP-scanned triplet conformations mentioned earlier. These multi-configurational calculations were performed with the ORCA 5.0 code [75] and the basis set remains unchanged at 6-31G(d,p).

## ACKNOWLEDGEMENTS

Y.R.P., N.P.K., R.G.H., and J.Y.-Z. were supported through the U.S. Department of Energy (DOE) under 2019030-SP DOE CalTech Sub S532207 (DE-SC0022089). D.M. and G.G. were supported by the Academy of Finland, grants 323996 and 332743. N.P.K. acknowledges support by the Hertz Fellowship and the National Science Foundation Graduate Research Fellowship Program under Grant No. DGE-1745301. We also thank Arghadip Koner and Kai Schwennicke for helpful discussions.

---

[1] D. D. Awschalom, R. Hanson, J. Wrachtrup, and B. B. Zhou, *Nature Photonics* **12**, 516 (2018).

[2] M. H. Abobeih, J. Randall, C. E. Bradley, H. P. Bartling, M. A. Bakker, M. J. Degen, M. Markham, D. J. Twitchen, and T. H. Taminiau, *Nature* **576**, 411 (2019).

[3] W. Pfaff, B. J. Hensen, H. Bernien, S. B. van Dam, M. S. Blok, T. H. Taminiau, M. J. Tiggelman, R. N. Schouten, M. Markham, D. J. Twitchen, and R. Hanson, *Science* **345**, 532 (2014).

[4] J. M. Taylor, P. Cappellaro, L. Childress, L. Jiang, D. Budker, P. R. Hemmer, A. Yacoby, R. Walsworth, and M. D. Lukin, *Nature Physics* **4**, 810 (2008).

[5] C. Degen, F. Reinhard, and P. Cappellaro, *Reviews of Modern Physics* **89**, 035002 (2017).

[6] B. C. Rose, D. Huang, Z.-H. Zhang, P. Stevenson, A. M. Tyryshkin, S. Sangtawesin, S. Srinivasan, L. Loudin, M. L. Markham, A. M. Edmonds, D. J. Twitchen, S. A. Lyon, and N. P. de Leon, *Science* **361**, 60 (2018).

[7] A. Gottscholl, M. Kianinia, V. Soltamov, S. Orlinskii, G. Mamin, C. Bradac, C. Kasper, K. Krambork, A. Sperlich, M. Toth, I. Aharonovich, and V. Dyakonov, *Nature Materials* **19**, 540 (2020).

[8] N. Chejanovsky, A. Mukherjee, J. Geng, Y.-C. Chen, Y. Kim, A. Denisenko, A. Finkler, T. Taniguchi, K. Watanabe, D. B. R. Dasari, P. Auburger, A. Gali, J. H. Smet, and J. Wrachtrup, *Nature Materials* **20**, 1079 (2021).

[9] A. Gaita-Ariño, F. Luis, S. Hill, and E. Coronado, *Nature Chemistry* **11**, 301 (2019).

[10] M. Atzori and R. Sessoli, *Journal of the American Chemical Society* **141**, 11339 (2019).

[11] M. R. Wasielewski, M. D. E. Forbes, N. L. Frank, K. Kowalski, G. D. Scholes, J. Yuen-Zhou, M. A. Baldo, D. E. Freedman, R. H. Goldsmith, T. Goodson, M. L. Kirk, J. K. McCusker, J. P. Ogilvie, D. A. Shultz, S. Stoll, and K. B. Whaley, *Nature Reviews Chemistry* **4**, 490 (2020).

[12] C.-J. Yu, S. von Kugelgen, D. W. Laorenza, and D. E. Freedman, *ACS Central Science* **7**, 712 (2021).

[13] D. W. Laorenza and D. E. Freedman, *Journal of the American Chemical Society* **144**, 21810 (2022).

[14] M. K. Wojnar, D. W. Laorenza, R. D. Schaller, and D. E. Freedman, *Journal of the American Chemical Society* **142**, 14826 (2020).

[15] S. L. Bayliss, D. W. Laorenza, P. J. Mintun, B. D. Kovos, D. E. Freedman, and D. D. Awschalom, *Science* **370**, 1309 (2020).

[16] M. S. Fataftah, S. L. Bayliss, D. W. Laorenza, X. Wang, B. T. Phelan, C. B. Wilson, P. J. Mintun, B. D. Kovos, M. R. Wasielewski, S. Han, M. S. Sherwin, D. D. Awschalom, and D. E. Freedman, *Journal of the Amer-*

ican Chemical Society **142**, 20400 (2020).

[17] R. Mirzoyan, N. P. Kazmierczak, and R. G. Hadt, *Chemistry – A European Journal* **27**, 9482 (2021).

[18] N. P. Kazmierczak, R. Mirzoyan, and R. G. Hadt, *Journal of the American Chemical Society* **143**, 17305 (2021).

[19] D. W. Laorenza, A. Kairalapova, S. L. Bayliss, T. Goldzak, S. M. Greene, L. R. Weiss, P. Deb, P. J. Mintun, K. A. Collins, D. D. Awschalom, T. C. Berkelbach, and D. E. Freedman, *Journal of the American Chemical Society* **143**, 21350 (2021).

[20] M. J. Amdur, K. R. Mullin, M. J. Waters, D. Pugnioni, M. K. Wojnar, M. Gu, L. Sun, P. H. Oyala, J. M. Rondinelli, and D. E. Freedman, *Chemical Science* **13**, 7034 (2022).

[21] S. Bayliss, P. Deb, D. Laorenza, M. Onizhuk, G. Galli, D. Freedman, and D. Awschalom, *Physical Review X* **12**, 031028 (2022).

[22] T. Goh, R. Pandharkar, and L. Gagliardi, *The Journal of Physical Chemistry A* **126**, 6329 (2022).

[23] N. P. Kazmierczak and R. G. Hadt, *Journal of the American Chemical Society* **144**, 20804 (2022).

[24] N. P. Kazmierczak, K. M. Luedcke, E. T. Gallmeier, and R. G. Hadt, *The Journal of Physical Chemistry Letters* **14**, 7658 (2023).

[25] K. R. Mullin, D. W. Laorenza, D. E. Freedman, and J. M. Rondinelli, *Physical Review Research* **5**, L042023 (2023).

[26] K. E. Smyser and J. D. Eaves, *Scientific Reports* **10**, 18480 (2020).

[27] S. Gorgon, K. Lv, J. Grüne, B. H. Drummond, W. K. Myers, G. Londi, G. Ricci, D. Valverde, C. Tonnelé, P. Murto, A. S. Romanov, D. Casanova, V. Dyakonov, A. Sperlich, D. Beljonne, Y. Olivier, F. Li, R. H. Friend, and E. W. Evans, *Nature* **620**, 538 (2023).

[28] J. R. Palmer, M. L. Williams, R. M. Young, K. R. Peinkofer, B. T. Phelan, M. D. Krzyaniak, and M. R. Wasielewski, *Journal of the American Chemical Society* **146**, 1089 (2024).

[29] A. Mena, S. K. Mann, A. Cowley-Semple, E. Bryan, S. Heutz, D. R. McCamey, M. Attwood, and S. L. Bayliss, Room-temperature optically detected coherent control of molecular spins (2024), arXiv:2402.07572 [quant-ph].

[30] H. Singh, N. D’Souza, K. Zhong, E. Druga, J. Oshiro, B. Blankenship, J. A. Reimer, J. D. Breeze, and A. Ajoy, Room-temperature quantum sensing with photoexcited triplet electrons in organic crystals (2024), arXiv:2402.13898 [quant-ph].

[31] M. W. Doherty, N. B. Manson, P. Delaney, F. Jelezko, J. Wrachtrup, and L. C. L. Hollenberg, *Physics Reports The nitrogen-vacancy colour centre in diamond*, **528**, 1 (2013).

[32] Y. Hattori, E. Michail, A. Schmiedel, M. Moos, M. Holzapfel, I. Krummenacher, H. Braunschweig, U. Müller, J. Pflaum, and C. Lambert, *Chemistry – A European Journal* **25**, 15463 (2019).

[33] S. Kimura, M. Uejima, W. Ota, T. Sato, S. Kusaka, R. Matsuda, H. Nishihara, and T. Kusamoto, *Journal of the American Chemical Society* **143**, 4329 (2021).

[34] M. B. S. Wonink, B. P. Corbet, A. A. Kulago, G. B. Boursalian, B. de Bruin, E. Otten, W. R. Browne, and B. L. Feringa, *Journal of the American Chemical Society* **143**, 18020 (2021).

[35] Z. Feng, Y. Chong, S. Tang, Y. Fang, Y. Zhao, J. Jiang, and X. Wang, *Chemical Science* **12**, 15151 (2021).

[36] B. Huang, H. Kang, C.-W. Zhang, X.-L. Zhao, X. Shi, and H.-B. Yang, *Communications Chemistry* **5**, 10.1038/s42004-022-00747-8 (2022).

[37] A. Abdurahman, J. Wang, Y. Zhao, P. Li, L. Shen, and Q. Peng, *Angewandte Chemie International Edition* **62**, e202300772 (2023).

[38] R. Matsuoka, S. Kimura, T. Miura, T. Ikoma, and T. Kusamoto, *Journal of the American Chemical Society* **145**, 13615 (2023).

[39] A. Abdurahman, L. Shen, J. Wang, M. Niu, P. Li, P. Qiming, J. Wang, and G. Lu, *A Highly Efficient Open-shell Singlet Luminescent Diradical with Strong Magnetoluminescence Properties* (2023).

[40] M. Abe, *Chemical Reviews* **113**, 7011 (2013).

[41] J. Casado, in *Physical Organic Chemistry of Quinodimethanes*, Topics in Current Chemistry Collections, edited by Y. Tobe and T. Kubo (Springer, Cham, 2017) pp. 209–248.

[42] T. Stuyver, B. Chen, T. Zeng, P. Geerlings, F. De Proft, and R. Hoffmann, *Chemical Reviews* **119**, 11291 (2019).

[43] P. Murto and H. Bronstein, *Journal of Materials Chemistry C* **10**, 7368 (2022).

[44] B. Prajapati, M. D. Ambhore, D.-K. Dang, P. J. Chmielewski, T. Lis, C. J. Gómez-García, P. M. Zimmerman, and M. Stępień, *Nature Chemistry* **15**, 1541 (2023).

[45] T. Khvorost, P. Wojcik, C. Chang, M. Calvillo, C. Dickerson, A. Krylov, and A. Alexandrova 10.26434/chemrxiv-2024-fmrnw-v2 (2024).

[46] C. E. Dickerson, H. Guo, G.-Z. Zhu, E. R. Hudson, J. R. Caram, W. C. Campbell, and A. N. Alexandrova, *The Journal of Physical Chemistry Letters* **12**, 3989 (2021).

[47] G.-Z. Zhu, D. Mitra, B. L. Augenbraun, C. E. Dickerson, M. J. Frim, G. Lao, Z. D. Lasner, A. N. Alexandrova, W. C. Campbell, J. R. Caram, J. M. Doyle, and E. R. Hudson, *Nature Chemistry* **14**, 995 (2022).

[48] T. J. Gately, R. A. Boto, M. J. Tauber, D. Casanova, and C. J. Bardeen, *The Journal of Physical Chemistry C* **127**, 4816 (2023).

[49] T. J. Penfold, E. Gindensperger, C. Daniel, and C. M. Marian, *Chemical Reviews* **118**, 6975 (2018).

[50] M. A. El-Sayed, *The Journal of Chemical Physics* **38**, 2834 (1963).

[51] T.-M. Hong and H.-F. Meng, *Physical Review B* **63**, 075206 (2001).

[52] J. Rybicki and M. Wohlgennannt, *Physical Review B* **79**, 153202 (2009).

[53] W. Barford, R. J. Bursill, and D. V. Makhov, *Physical Review B* **81**, 035206 (2010).

[54] Z. G. Yu, *Physical Review B* **85**, 115201 (2012).

[55] R. Pariser and R. G. Parr, *The Journal of Chemical Physics* **21**, 767 (1953).

[56] J. A. Pople, *Transactions of the Faraday Society* **49**, 1375 (1953).

[57] J. Linderberg and Y. öhrn, *The Journal of Chemical Physics* **49**, 716 (1968).

[58] H. C. Longuet-Higgins, *The Journal of Chemical Physics* **18**, 265 (1950).

[59] M. J. S. Dewar and H. C. Longuet-Higgins, *Proceedings of the Physical Society. Section A* **67**, 795 (1954).

[60] H. C. Longuet-Higgins and J. A. Pople, *Proceedings of the Physical Society. Section A* **68**, 591 (1955).

[61] T. J. H. Hele, in *Physical Chemistry of Semiconductor Materials and Interfaces XX*, Vol. 11799, edited by A. J. Musser and D. Baran, International Society for Optics and Photonics (SPIE, 2021) p. 117991A.

[62] A. Szabo and N. S. Ostlund, *Modern Quantum Chemistry: Introduction to Advanced Electronic Structure Theory* (Dover Publications, 1989).

[63] R. Pariser, *The Journal of Chemical Physics* **24**, 250 (1956).

[64] T. J. H. Hele, E. G. Fuemmeler, S. N. Sanders, E. Kumarasamy, M. Y. Sfeir, L. M. Campos, and N. Ananth, *The Journal of Physical Chemistry A* **123**, 2527 (2019).

[65] A. Abdurahman, T. J. H. Hele, Q. Gu, J. Zhang, Q. Peng, M. Zhang, R. H. Friend, F. Li, and E. W. Evans, *Nature Materials* **19**, 1224 (2020).

[66] L. Salem and C. Rowland, *Angewandte Chemie International Edition in English* **11**, 92 (1972).

[67] N. M. Atherton, Principles of Electron Spin Resonance (Ellis Horwood, 1993) Chap. High-spin systems, pp. 224–263.

[68] R. Englman and J. Jortner, *Molecular Physics* **18**, 145 (1970).

[69] V. Gamero, D. Velasco, S. Latorre, F. López-Calahorra, E. Brillás, and L. Juliá, *Tetrahedron Letters* **47**, 2305 (2006).

[70] These values were calculated using the Q-Chem package (version 6.0.2) [73]. For the same computation on the Gaussian16 software [?], the respective values were  $-0.005$  eV and  $+0.001$  eV at  $\theta = 90^\circ$ , and  $-0.009$  eV and  $+0.001$  eV at  $\theta = 110^\circ$ .

[71] A. D. Laurent and D. Jacquemin, *International Journal of Quantum Chemistry* **113**, 2019 (2013).

[72] M. A. Nielsen and I. L. Chuang, Quantum Computation and Quantum Information (Cambridge University Press, 2010) Chap. Quantum circuits, pp. 171–215, 10th Anniversary ed.

[73] E. Epifanovsky, A. T. B. Gilbert, X. Feng, J. Lee, Y. Mao, N. Mardirossian, P. Pokhilko, A. F. White, M. P. Coons, A. L. Dempwolff, Z. Gan, D. Hait, P. R. Horn, L. D. Jacobson, I. Kaliman, J. Kussmann, A. W. Lange, K. U. Lao, D. S. Levine, J. Liu, S. C. McKenzie, A. F. Morrison, K. D. Nanda, F. Plasser, D. R. Rehn, M. L. Vidal, Z.-Q. You, Y. Zhu, B. Alam, B. J. Albrecht, A. Aldossary, E. Alguire, J. H. Andersen, V. Athavale, D. Barton, K. Begam, A. Behn, N. Bellonzi, Y. A. Bernard, E. J. Berquist, H. G. A. Burton, A. Carreras, K. Carter-Fenk, R. Chakraborty, A. D. Chien, K. D. Closser, V. Cofer-Shabica, S. Dasgupta, M. de Wergifosse, J. Deng, M. Diedenhofen, H. Do, S. Ehler, P.-T. Fang, S. Fatehi, Q. Feng, T. Friedhoff, J. Gayvert, Q. Ge, G. Gidofalvi, M. Goldey, J. Gomes, C. E. González-Espinoza, S. Gulania, A. O. Gunina, M. W. D. Hanson-Heine, P. H. P. Harbach, A. Hauser, M. F. Herbst, M. Hernández Vera, M. Hodecker, Z. C. Holden, S. Houck, X. Huang, K. Hui, B. C. Huynh, M. Ivanov, Á. Jász, H. Ji, H. Jiang, B. Kaduk, S. Kähler, K. Khistyayev, J. Kim, G. Kis, P. Klunzinger, Z. Koczor-Benda, J. H. Koh, D. Kosenkov, L. Koulias, T. Kus, I. Ladjánszki, A. Landau, K. V. Lawler, D. Lefrancois, S. Lehtola, R. R. Li, Y.-P. Li, J. Liang, M. Liebenthal, H.-H. Lin, Y.-S. Lin, F. Liu, K.-Y. Liu, M. Loipersberger, A. Luenser, A. Manjanath, P. Manohar, E. Mansoor, S. F. Manzer, S.-P. Mao, A. V. Marenich, T. Markovich, S. Mason, S. A. Mauerer, P. F. McLaughlin, M. F. S. J. Menger, J.-M. Mewes, S. A. Mewes, P. Morganate, J. W. Mullinax, K. J. Oosterbaan, G. Paran, A. C. Paul, S. K. Paul, F. Pavošević, Z. Pei, S. Prager, E. I. Proynov, Á. Rák, E. Ramos-Cordoba, B. Rana, A. E. Rask, A. Rettig, R. M. Richard, F. Rob, E. Rossumme, T. Scheele, M. Scheurer, M. Schneider, N. Sergueev, S. M. Sharada, W. Skomorowski, D. W. Small, C. J. Stein, Y.-C. Su, E. J. Sundstrom, Z. Tao, J. Thirman, G. J. Tornai, T. Tsuchimochi, N. M. Tubman, S. P. Veccham, O. Vydrov, J. Wenzel, J. Witte, A. Yamada, K. Yao, S. Yeganeh, S. R. Yost, A. Zech, I. Y. Zhang, X. Zhang, Y. Zhang, D. Zuev, A. Aspuru-Guzik, A. T. Bell, N. A. Besley, K. B. Bravaya, B. R. Brooks, D. Casanova, J.-D. Chai, S. Coriani, C. J. Cramer, G. Cserey, A. E. DePrince, 3rd, R. A. DiStasio, Jr, A. Dreuw, B. D. Dunietz, T. R. Furlani, W. A. Goddard, 3rd, S. Hammes-Schiffer, T. Head-Gordon, W. J. Hehre, C.-P. Hsu, T.-C. Jagau, Y. Jung, A. Klamt, J. Kong, D. S. Lambrecht, W. Liang, N. J. Mayhall, C. W. McCurdy, J. B. Neaton, C. Ochsenfeld, J. A. Parkhill, R. Peverati, V. A. Rassolov, Y. Shao, L. V. Slipchenko, T. Stauch, R. P. Steele, J. E. Subotnik, A. J. W. Thom, A. Tkatchenko, D. G. Truhlar, T. Van Voorhis, T. A. Wesolowski, K. B. Whaley, H. L. Woodcock, 3rd, P. M. Zimmerman, S. Faraji, P. M. W. Gill, M. Head-Gordon, J. M. Herbert, and A. I. Krylov, *The Journal of Chemical Physics* **155**, 084801 (2021).

[74] K. Yamaguchi, F. Jensen, A. Dorigo, and K. N. Houk, *Chemical Physics Letters* **149**, 537 (1988).

[75] F. Neese, *WIREs Computational Molecular Science* **12**, e1606 (2022).